J Nanopart Res (2008) 10:599–612
DOI 10.1007/s11051-007-9290-y

RESEARCH PAPER

In-situ characterization of dispersion stability of WO_3 nanoparticles and nanowires

Mehmet Kozan · Jyothish Thangala · Rahel Bogale · M. Pinar Mengüç · Mahendra K. Sunkara

Received: 14 November 2006 / Accepted: 7 August 2007 / Published online: 24 August 2007

Abstract The stability of tungsten trioxide (WO_3) suspensions in various common polar solvents such as water, acetone, isopropanol (IPA), ethanol, 1-methoxy-2-propanol (1M-2P) and N,N-dimethylformamide (DMF) was investigated. The morphology of WO_3 aggregates formed by irregular nanoparticles ($d \sim 40$ nm, with 1 μm nominal diameter compact aggregates) and by nanowires of different types (uneven, single or bundled in diameter) and dimensions (nominal lengths of 2, 4, 6, and 10 μm) were described by means of the small angle static light scattering and the elliptically polarized light scattering (EPLS) techniques. Aggregation of low aspect ratio (bundled) 2 μm nanowires monitored through the change in spatial extent of the aggregate was found to be minimal (i.e., radius of gyration, $R_g \sim$ 1.8–2.2 μm in 1-methoxy-2-propanol), with a minimal change in aggregate structure (i.e., fractal dimension, $D_f \sim 1.8$–1.9 in 1-methoxy-2-propanol) in a time period of about 1 week. Fractal dimension was found to be the lowest for the low aspect ratio nanowires when suspended in N,N-dimethylformamide ($D_f \sim 1.4$). Aggregates of very high aspect ratio single nanowires ($L/D \sim 250$ with 10 μm nominal length) were also observed to form stable dispersions in a period of about a week. Aggregate structures that would lead to observed fractal dimensions were proposed. Information on how well inorganic nanowires are dispersed in various solvents is based singly on the time consuming and intrusive advanced microscopy analyses (such as SEM and TEM) in the literature, and without any reference to the underlying structures. To our knowledge, this study is the first attempt for in-situ description of the underlying causes, such as aggregate morphologies, aggregation rates and solvent types, of the observed dispersion and sedimentation behaviors of inorganic nanowires that were not subjected to any surface treatment or functionalization.

Keywords Nanowire · Aggregation · Colloid stability · Fractal dimension · Small angle static light scattering · Elliptically polarized light scattering · Theory · Experiment

M. Kozan · M. P. Mengüç (✉)
Department of Mechanical Engineering, University of Kentucky, Lexington, KY 40506, USA
e-mail: menguc@engr.uky.edu

J. Thangala · R. Bogale · M. K. Sunkara
Department of Chemical Engineering, University of Louisville, Louisville, KY 40292, USA

Introduction

Dispersion of nanoparticles in a variety of solvents is important for applications involving cosmetics, pharmaceuticals, paints, inks, composites and catalysts. However, this can be extremely difficult as nanoparticles tend to agglomerate fairly quickly, especially without some type of a dispersing agent (Hou et al.

2006). Nanomaterial powders are dispersed in solvents by breaking their agglomerates using mechanical milling or ultrasonication, and are stabilized using surfactants, polymer coatings or by the use of pH (Lee et al. 2003; Saltiel et al. 2004). The stability of these colloidal systems is generally described by the DLVO-type electric double layer repulsion counteracting against the van der Waals attraction (Bushell et al. 2002). Recently, there has been significant progress in the synthesis of one dimensional nanowires, the cylindrically shaped materials with high aspect ratios. Typical diameters of these nanowires range between 1–100 nm and lengths range between 1–10 μm. Due to their high aspect ratios, the agglomeration behavior of nanowires within solvents is expected to be different than that of spherical nanoparticles. Only recently, a few studies discussed the dispersion of nanowires in polar solvents (Nicolosi et al. 2005; Deepak et al. 2006).

The process of aggregation is integral to how colloid systems evolve, and it is important to understand the structure and properties of the resulting clusters to better control many important industrial processes (Sorensen 2001; Filippov et al. 2000). Extensive in-situ agglomeration studies are available on particles, which consist of a number of small, nearly spherical particles (called spherules, primary particles or monomers) which join together to form tenuous clusters (called floccules, flocs or aggregates). Such geometries usually cannot successfully be approximated as dense porous spheres or other simple shapes and conventional geometrical tools, but are statistically described in terms of the concepts of fractal geometry (Filippov et al. 2000; Brasil et al. 1999). The research on fractal aggregates formed by primary particles in shapes other than spheres, however, is scarce.

Characterization of colloidal particles can be achieved using advanced microscopy techniques, such as SEM, TEM or AFM. However, off-line analysis techniques such as SEM have the potential risk of modifying aggregate structure during handling or biasing aggregate orientation on a slide. The small angle static light scattering technique, on the other hand, is a powerful in-situ characterization tool that can produce accurate results rapidly (Bushell et al. 2002; Sorensen 1997). Static light scattering technique samples large numbers of aggregates at the same time, and provides a statistical average of the aggregate mixture. Elliptically polarized light scattering (EPLS) techniques are also based on static light scattering and provide more details about the size, size distribution, shape and structure of particles or their agglomerates. Details of the EPLS technique used in this study can be found in (Govindan et al. 1995; Mengüç and Manickavasagam 1998; Aslan et al. 2006).

In the present study, we studied the effect of geometry of nanomaterials on the stability of the dispersions in various commonly used polar solvents such as water, ethanol, 1-methoxy-2-propanol (1M-2P) and N,N-dimethylformamide (DMF). Tungsten trioxide (WO_3) nanomaterials were used to compare the dispersion behavior of nanowires with that of irregular nanoparticles. The morphology of WO_3 aggregates formed by irregular nanoparticles and nanowires were determined by means of the small angle static light scattering and the EPLS techniques. Scattered light intensities were used to describe spatial extent (or radius of gyration, R_g) of the aggregates, their fractal dimension (D_f), and the change in aggregate structure as a function of time and solvent type. The shapes of irregular nanoparticles and nanowires were also verified using SEM images.

Theory

Statistical scaling law

Fractal aggregates are scale invariant, i.e., within limits they appear the same when viewed over a range of scales (Sorensen 2001). The mathematical description of a fractal aggregate is simple and can be expressed as

$$N = k_g(R_g/r_o)^{D_f} \quad (1)$$

where N is the number of primary particles, R_g is the radius of gyration of the aggregate, r_o is the radius of primary particles, k_g is the structure pre-factor and D_f is the fractal dimension of the aggregate.

Aggregates of fine particles, such as nanowires used in this study, are not fractals in the strict sense of the word. Since their scaling is only observed over a finite range of length scales, these aggregates should be called “natural fractals” (Bushell et al. 2002). In a rare study of aggregates formed by non-spherical primary particles, fractal nature was established for a

system of large carbon rods ($\sim$140 μm long, 35 μm in diameter) confined to a two dimensional surface using image analysis (Vincze et al. 1997). Fractal behavior was also observed for aggregates of carbon nanotubes (Chen et al. 2004; Saltiel et al. 2005).

Determination of structure from light scattering experiments is based on the Rayleigh-Gans-Debye (RGD) theory. The basic approach of RGD theory is to model the scattering body as a collection of Rayleigh scatterers that do not interact with each other. If also the suspension is sufficiently dilute, the interaction between aggregates can be described as independent scattering (Modest 1993), and the scattered intensity is proportional to $n_a N^2$, where n_a is the number density of aggregates in the solution (Sorensen 2001). Even in cases where the Rayleigh scatterers are too close to be independent and the primary particles are not small compared to the wavelength of incident light, RGD theory still provides conservative limits for the fractal analysis of scattered intensity profiles given the fact that D_f is determined on a log-log plot of scattered intensity as a function of scattering angle, from the slope of the scattering curve rather than of its absolute value.

Although, real processes that form natural fractals may impose more limitations, in a real physical process, fractal dimension for most aggregates assume a value within the range (Bushell et al. 2002)

$$1 \leq D_f \leq 3 \tag{2}$$

The $1.8 < D_f < 2.1$ range is universally agreed in the literature for cluster–cluster type aggregations (CCA) (Bushell et al. 2002). Higher fractal dimensions are also reported in the literature e.g. for hematite aggregates in the range $2.3 < D_f < 2.9$ (Raper and Amal 1993). The lower end corresponds to diffusion limited aggregation and the upper end to reaction limited aggregation processes in this and in the universal cluster-cluster aggregation range mentioned above. However, there is no "universal" agreement on the limits of particle–cluster aggregation (PCA) mechanism. The most commonly referred value is $D_f = 2.5$ for diffusion limited PCA, although higher values have also been reported (Brasil et al. 2001). Polarizable clusters, on the other hand, were shown to have linear aggregates with much lower fractal dimension values ($D_f \sim 1.4$) (Jullien 1986).

Determining aggregate morphology from the angular scattered intensity pattern

In the case of small angle static light scattering experiments, overall variation at small q is entirely due to aggregate structure effects $S(q)$, hence $I(q) \propto S(q)$. The aggregate structure factor, in the case of RGD scattering has the following form

$$S(q) \propto q^{-D_f} \tag{3}$$

where q given by

$$q = |\vec{q}| = \frac{4\pi n}{\lambda_0} \sin\left(\frac{\theta}{2}\right) \tag{4}$$

is the magnitude of the scattering wave vector, and n is the refractive index of the dispersion medium, λ_o is the in vacuum wavelength and θ is the angle at which the radiation is scattered (Bushell et al. 2002). The overall variation in intensity at large q, however, is due to primary particles and scattering is described by the Porod regime. In this region the length scale of scattering experiment ($\lambda_o \propto q^{-1}$) can resolve the size of individual monomers (Sorensen 1997)—a topic we have investigated in another study (Kozan and Mengüç 2007).

The above proportionality for $S(q)$ can be used to determine D_f from the negative slope of the linear region of a log-log plot of I versus q measurement in the range (Bushell et al. 2002)

$$\frac{1}{R_g} \ll q \ll \frac{1}{r_0} \tag{5}$$

R_g is best determined from analysis of scattering in the Guinier regime, where $qR_g < 1$, which corresponds to $I(0)/I(q) < 4/3$ according to the Guinier equation expressed as (Sorensen 2001)

$$\frac{I(0)}{I(q)} \cong 1 + \frac{1}{3} R_g^2 q^2 \tag{6}$$

Although the plot of $I(0)/I(q)$ versus q^2 remains linear (the slope yields $R_g^2/3$) well beyond these limits for systems with polydispersity in aggregate size (Sorensen 2001), this relation should be used cautiously and only when there is sufficient amount of measurements at low q.

An important note on experiments based on the small angle light scattering techniques is that they inadvertently detect scattering from an ensemble of

cluster sizes. The polydispersity in the cluster size causes the shape of the structure factor to be different than that for a single cluster size (Sorensen 2001). A narrow size distribution causes a rapid transition, whereas a wide size distribution causes a slow transition to the fractal scattering region (Bushell et al. 2002). The scattered light intensity, I_{vv}, when plotted against scattering vector, q, hence gives an effective structure factor for the ensemble, S_{eff}. The R_g measured by the experiment is then the average radius of gyration, $\langle R_g \rangle$ (Sorensen 2001). Polydispersity in primary particle size, on the other hand, causes the sharp ripples observed in the Porod regime to fade away, however the q^{-4} dependency originating from the Lorenz-Mie spheres remains (Sorensen 1997; Dimon et al. 1986).

The intensity and polarization state of light can also be described by four Stokes parameters in the form of a column vector [K] (Govindan et al. 1995; Mengüç and Manickavasagam 1998; Aslan et al. 2006). These four parameters can be obtained by using a set of filters in front of the beam. The incident and scattered Stokes vectors are related through the amplitude scattering matrix [S].

$$[K]_s = [S][K]_i \tag{7}$$

Elements of the scattering matrix S_{ij} provide information about the randomly oriented particles in the scattering media. EPLS is a powerful tool to identify particle morphology and is used to determine particle size and shape for conventional, as well as fractal geometries.

Experimental determination of fractal dimension from EPLS using scattering matrix elements has been illustrated in a recent work (Saltiel et al. 2004). Structure factor is expressed in terms of two of the scattering matrix elements

$$S(q) = S_{11} - S_{12} \tag{8}$$

The fractal dimension is then determined in a similar manner from the negative slope of the linear region of a log-log plot of S_{11}–S_{12} versus q measurement. This was also shown to be a viable method in determining the fractal dimension of aggregates of one dimensional geometries, such as single and multi-walled carbon nanotubes (Chen et al. 2004; Saltiel et al. 2005).

Nanowire synthesis and sample preparation

Bulk synthesis of WO_3 nanowires was carried out in a Hot Filament CVD reactor shown in Fig. 1 using a procedure described in (Vaddiraju et al. 2003). A detailed outline of the setup and the synthesis procedure is reported elsewhere (Thangala et al. 2007). Briefly, two different sets of experimental conditions were used for synthesis of nanowires, i.e., "with" and "without" heating the quartz tube by means of a furnace around it. In the first set of experiments, the tube furnace was heated to 800 °C. Argon and air gas mixtures at a ratio of 100/0.4 sccm were used. Also, the tungsten filament was heated to a temperature of about 1690 °C. In the second set of experiments, no furnace heating was used. In this case, the radiation from the tungsten filament (1690 °C) heated the quartz tube to temperatures around 500–600 °C. Air was used as feed gas at a flow rate of 11 sccm. These experiments typically resulted in the deposition of "bundled" nanowires;

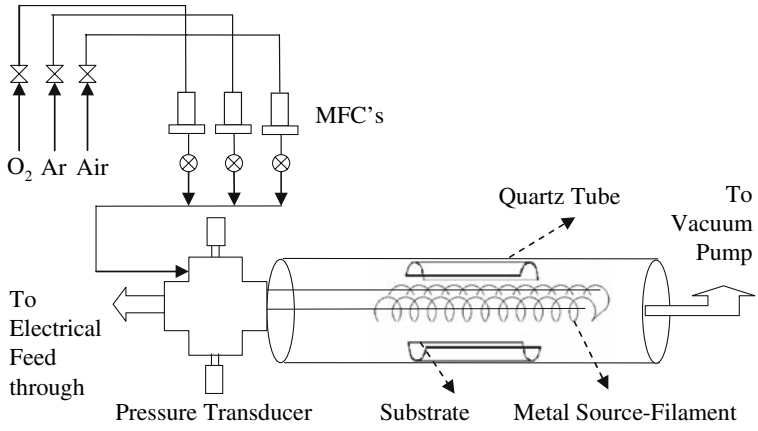

Fig. 1 Schematic of the scale up Hot Filament CVD reactor with tungsten filament inside the vacuum chamber

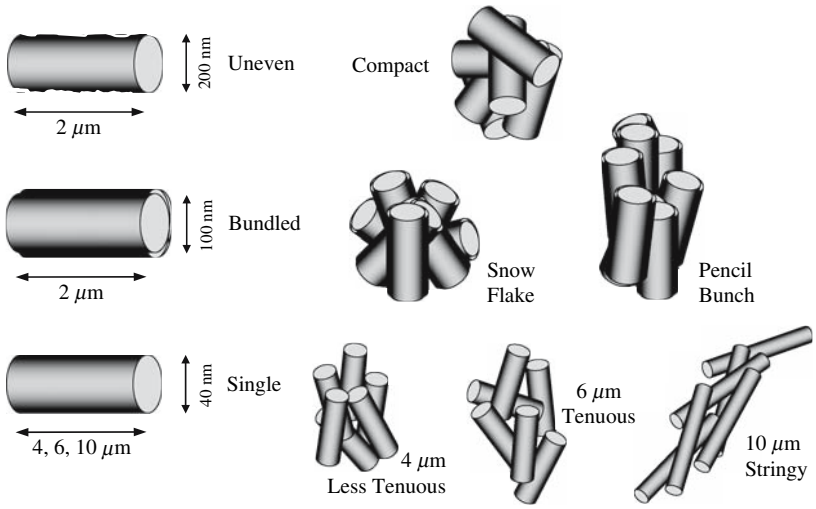

Fig. 2 Classification used in this study is based on appearance of nanowires and their aggregates, structures shown here are with approximate dimensions (not to scale)

Table 1 Summary of synthesis and dispersion conditions of WO_3 nanowires and nanoparticles

Sample	Nominal Dia., (nm)	Synthesis conditions	Solvent
2 μm wires	200 (uneven)	T_s = 900 °C; 1.5 sccm O_2 ; 100 sccm Ar; T_f = 1690 °C	EtOH
2 μm wires	100 (bundled)	T_s = 600 °C; 11 sccm air; T_f = 1690 °C	1M-2P, DMF, H_2O
4, 6, 10 μm wires	40 (single)	T_s = 800 °C; 0.4 sccm air; 100 sccm Ar; T_f = 1690 °C	Acetone, IPA
Nanoparticles	40	Commercial powder	EtOH, Acetone

whereas by heating the furnace walls more uniform "single" nanowires or nanowires with large "uneven" diameters (Fig. 2) were obtained as a result of different substrate temperatures and gas flow rates. In Fig. 2 we also suggest some possible aggregate structures based on our discussions below. Table 1 presents a summary of experimental conditions used in all three sets.

WO_3 nanowires that resulted on quartz slides placed inside the boats (in complete contact with the quartz boat) were carefully scrapped off without scratching the surface of the substrate. The nanowire powder thus obtained was dispersed into different solvents. Once the nanowires or irregular nanoparticles were combined with the selected solvent, ultrasonication (UP200S Ultrasonic Processor) was used to disperse the nanomaterial in the solution. High power ultrasonication using an ultrasonic horn (24 kHz, 200 W) was performed for about 2 min followed by the use of a low power ultrasonic bath for about 15 min to further disperse the nanowires. In the case of bundled nanowires, solutions were left on the shelf in glass vials for a few hours after the ultrasonication process. Thicker wires and their agglomerates sedimented and the well-dispersed portion of the solution was taken out into a new glass vial. The sediment was collected and the weight percent of the dispersed nanowires in the solution was calculated.

Solutions containing single nanowires which had a nominal diameter of about 40 nm were then subjected to high power ultrasonic horn for different ultrasonication periods to obtain nominal lengths of 4, 6, and 10 μm. Nanowires with large uneven diameters (~200 nm) were ~2 μm in length. Nanowire bundles prepared without heating the reactor walls, on the other hand, were found to be about 100 nm in diameter with a nominal length of about 2 μm. Irregular nanoparticle solutions were prepared using commercially available 40 nm diameter WO_3 nanoparticles (Aldrich, Inc.).

Experimental setup

The experimental setup used for EPLS measurements in this study was first proposed by (Govindan et al. 1995; Mengüç and Manickavasagam 1998) and later

modified and improved by (Aslan et al. 2006). The setup was used to measure scattering matrix elements, but was modified to also carry out the vertically polarized incident and detected light (I_{vv}) measurements. Of the six scattering elements available, only S_{11} and S_{12} elements were utilized in this study to demonstrate the capability of the system in determining the fractal dimension. For the I_{vv} measurements the quarter wave plate located after the polarizer in the path of the incident beam, and the quarter wave plate located before the polarizer in the path of the scattered beam were removed.

In-situ agglomeration characterization procedure

Just as for light scattering for the purpose of particle sizing, small angle static light scattering is only good for rather dilute samples (Bushell et al. 2002), where the interaction between particles can be described as independent scattering (Modest 1993). The samples which arrived as suspensions of WO_3 irregular nanoparticles and WO_3 nanowires were diluted to volume fractions in the order of $f_v = 10^{-6}$ to ensure independent scattering behavior. Measurements performed on single nanowire suspensions in ethanol, propanol, and acetone were performed while the diluted sample was stirred gently with a small size stirrer set at a low rpm. The paddle type stirrer (IKA model RW11) was immersed in the liquid away from the path of the laser beam close to the liquid surface.

I_{vv} measurements were first performed for suspensions of WO_3 ($\rho = 7.16$ g/cm^3, $m = 1.98 + i0.009$) nanoparticles and uneven WO_3 nanowires in ethanol ($\rho = 0.789$ g/cm^3, $n = 1.36$). Samples were carefully drawn out of their bottles with a Fisherbrand Finnpipette and transferred into sample holder containing 100 mL of the solvent used. After gently stirring the suspension, the sample cell was placed in the experimental setup. Although the samples were dispersed, or broken to desired length by means of ultrasonication in the synthesis and sample preparation stage, no ultrasonication was used on any WO_3 samples during light scattering measurements. Measurement of I_{vv} intensity was performed starting from scattering angle $\theta = 3°$. Measurements on single WO_3 nanowires with higher average lengths of 4 and 6 μm in propanol ($\rho = 0.804$ g/cm^3, $n = 1.377$) and of 10 μm in acetone ($\rho = 0.791$ g/cm^3, $n = 1.357$) were performed following the same procedure.

Continuous plots are the average of two measurements for all figures given below unless otherwise is stated. Continuous measurements were performed at a low sweeping speed with PMT readings of 10 counts/s. The majority of experiments were performed between $\theta = 3°$–$90°$ and lasted for 174 s, except for the two experiments with ethanol (for irregular nanoparticles and uneven nanowires) where measurements between $\theta = 3°$–$145°$ lasted for 284 s. All samples except these two experiments with ethanol were also subjected to measurements at discrete scattering angles, with 1° increments up to about $\theta = 10°$ and higher increments thereafter. Incremental measurements on single nanowires of all lengths (4, 6, and 10 μm) were taken for 15 s (150 readings at each point) at discrete scattering angles and for 10 s (100 readings) on bundled nanowires. For the incremental measurements, the readings fluctuated evenly around a mean intensity at each discrete angle. Relative variance at low q, where detected intensities were the highest was negligible—especially on a log-log plot—but increased considerably at the last few data points of very high q. A similar behavior, i.e., higher noise at high q compared to that at lower values of q, was also observed for continuous measurements.

EPLS measurements as well as I_{vv} measurements were performed with bundled WO_3 nanowires suspended in three different solvents: 1-methoxy-2-propanol ($\rho = 0.921$ g/cm^3, $n = 1.403$), distilled water ($\rho = 1.0$ g/cm^3, $n = 1.333$), and N,N-dimethylformamide ($\rho = 0.948$ g/cm^3, $n = 1.428$) with 0.1 wt.%. These samples were prepared from their respective concentrated suspensions of 0.7 wt.%, 0.5 wt.%, and 0.4 wt.%. As for the I_{vv} measurements for uneven nanowires and irregular nanoparticles, all samples were diluted to volume fractions of the order of $f_v = 10^{-6}$ to ensure independent scattering behavior. EPLS measurements were carried out with 5° increments between $\theta = 25°$–$145°$, and for six different combinations of polarizer and retarder angles. EPLS and I_{vv} measurements on the diluted samples of bundled nanowires were performed *without* any stirring.

Good experimental practices demand the standardization of the measurements from this more elaborate setup by calibrating it using known results. This was

done by preparing a suspension of 450 nm average diameter latex spheres in distilled water, and comparing experimentally measured scattering matrix elements with those from the Lorenz-Mie scattering theory for homogeneous spheres of the same size and optical properties (Kozan 2007). Latex sample was carefully drawn from its bottle (Duke Scientific 5,045A, $\rho = 1.05$ g/cm^3, $n = 1.59$) with a Fisherbrand Finnpipette and diluted to a volume fraction of $f_v = 1.1 \times 10^{-6}$ followed by ultrasonication at a moderate power for several minutes.

Results and discussion

SEM images showing aggregates of irregular WO_3 nanoparticles and bundled nanowires are given in Fig. 3. Compact spherical aggregates formed by irregular WO_3 nanoparticles are seen in Fig. 3a. The primary particles forming the compact spherical aggregates seem to have different shapes and some size distribution, however, can safely be approximated as spherules for all general purposes with a radius of $r_o = 20$ nm. Using the procedure mentioned above, commercial WO_3 nanoparticle powders were suspended and ultrasonicated. SEM images of particles sedimented from the dispersion were taken. Some compact spherical aggregates seen in the figure were probably formed during the commercial production stage. Initially, their size was much lower (as obtained powders) and the shapes were not as spherical as shown in Fig. 3a, as observed from SEM analyses. This implies the continuation of an aggregation process in which spherical clusters continue to grow (e.g., as irregular nanoparticles or clusters stick on the surface). We never tried to re-disperse these aggregates; although, our previous experience with commercially obtained titania powders is that the aggregates could be broken into smaller clusters with prolonged ultrasonication.

Bundled WO_3 nanowires seen in Fig. 3b also have a wide distribution in diameter and length. SEM images given in Fig. 4 for single WO_3 nanowires of 10, 6, and 4 μm average length ($r_o \sim 20$ nm for all) were obtained by using the ultrasonic horn for a period of 5, 20, and 60 min, respectively. Figure 4d corresponds to the nanowires of uneven diameter. Different process conditions during chemical synthesis yield different nanowires (e.g., uneven or bundled), and depending on the power of ultrasonication used to prepare the nanowires, their aggregates can break up and then re-aggregate in the suspension. The 2 μm average length bundled WO_3 nanowires, therefore, are expected to form different aggregate structures than uneven nanowires of a similar average length. For both nanowire samples as well as for irregular nanoparticles, $\lambda_o = 632$ nm and $r_o = 20$ nm were used in the I_{vv} versus qr_o plots to consistently compare all measurements.

Figure 5a shows the I_{vv} versus q measurements corresponding to the compact spherical aggregates of WO_3 nanoparticles and aggregates of uneven WO_3 nanowires, both suspended in ethanol at $f_v = 1.1 \times 10^{-6}$. Initial concentration of both suspensions was 1.0 wt.% before dilution. Experimental plots are the average of two measurements performed for scattering angles between $\theta = 3°$–$145°$. Measurements are normalized by the highest intensity attained at $\theta = 3°$ for comparative purposes.

I_{vv} intensity profile for WO_3 nanoparticles in Fig. 5a perfectly follows the behavior of a fractal aggregate. The constant intensity observed in Rayleigh regime is followed by the transition into the Guinier regime which ends at about $qr_o = 0.023$ corresponding to scattering angle $\theta = 5°$. The linear behavior in the fractal scattering region continues until $qr_o = 0.124$ or $\theta = 27°$, after which point the

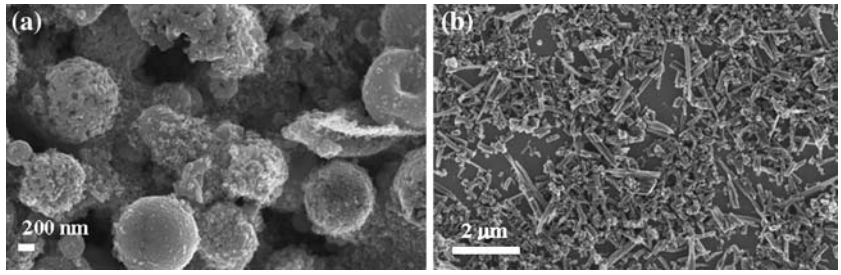

Fig. 3 SEM images of aggregates of (**a**) irregular WO_3 nanoparticles and (**b**) bundled WO_3 nanowires of 2 μm average length

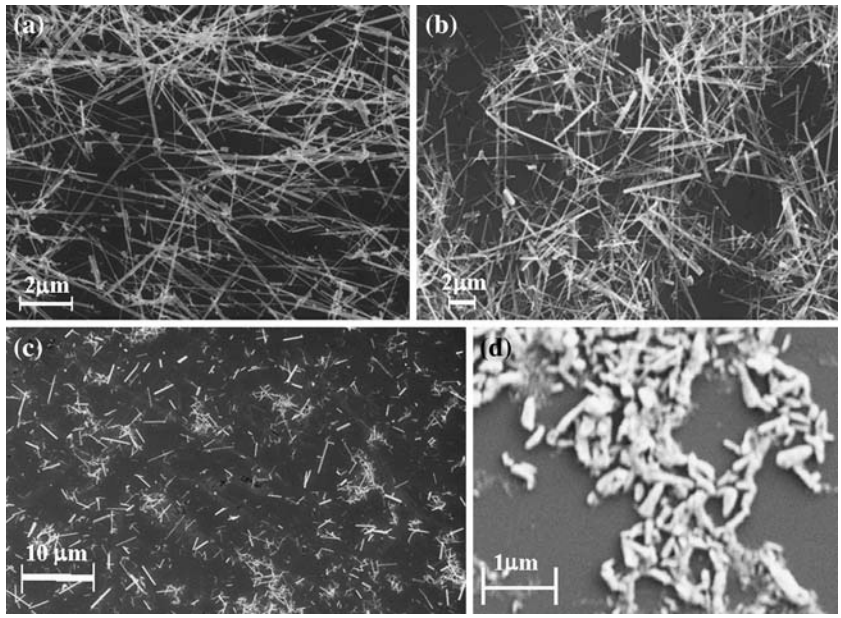

Fig. 4 SEM images of aggregates of single WO_3 nanowires ($d \sim 40$ nm) with 10, 6, and 4 μm average length as a result of (**a**) 5 min, (**b**) 20 min, and (**c**) 1 hour of ultrasonication, respectively. (**d**) Uneven nanowires with ~2 μm average length ($d \sim 200$ nm)

first ripples is observed reminiscent of the Porod regime, which is also due to increased noise. However, polydispersity in the suspension causes the rapid variations in intensity at high qr_o to be smoothed out. There is a wide linear region in this and the rest of the figures in this study (including incremental measurements) that we confine our fractal analysis to regions away from the onset of these ripples in the continuous measurements. $D_f = 2.59$ was found from the slope of the fractal scattering region by making a linear fit on data points between $\theta = 5°–25°$. As we will discuss below, continuous scattered intensity profiles tend to result in slightly higher D_f estimates, and should be used cautiously. This is due to PMT saturation at smaller angles (higher scattered intensity) which cause an overshoot in readings at subsequent angles.

A similar behavior is observed for uneven WO_3 nanowires of 2 μm average length, opening the door for a fractal description of the nanowire aggregates. The transition from Guinier region to fractal scattering region as well as the onset of Porod region corresponds to about the same scattering angles as for WO_3 nanoparticles. $D_f = 2.32$ was found from the slope of the fractal scattering region for WO_3 nanowires by making a linear fit on data points between $\theta = 5°$-$35°$.

The fractal dimension observed for the irregular WO_3 nanoparticle sample in Fig. 5a is close to the value of 2.5 mentioned above for the PCA mechanism, but the SEM picture of the sediment phase comprises mainly of compact spherical aggregates (clusters) and very few particles. Our observations via the SEM images have implied an increase in size and sphericity of the compact spherical aggregates in time, as discussed for Fig. 3a above, due possibly to sticking of irregular nanoparticles on the cluster surface. A more precise description of the underlying mechanism during which compact spherical aggregates were formed by nanoparticles, however, warrants further research (e.g., by use of well defined spherical nanoparticles as in (Raper and Amal 1993)). The fractal dimension for uneven WO_3 nanowires, on the other hand, is slightly higher than the value of 2.1 realized for reaction limited (slow) CCA mechanism. We provide further analysis which substantiates the slow aggregation rate of uneven nanowires by investigating their shelf life in (Kozan and Mengüç 2007). Nevertheless, it should be noted that the lower slope of uneven nanowire aggregates as opposed to that of irregular nanoparticles is expected since the nanowire aggregates do not form compact spherical structures as seen from the SEM images.

A plot of $I_{ref}/I(q)$ versus q^2 is given in Fig. 5b for the same aggregates of irregular nanoparticles and uneven nanowires in ethanol. Using the Guinier equation above, the linear fits between $\theta = 6°–14°$

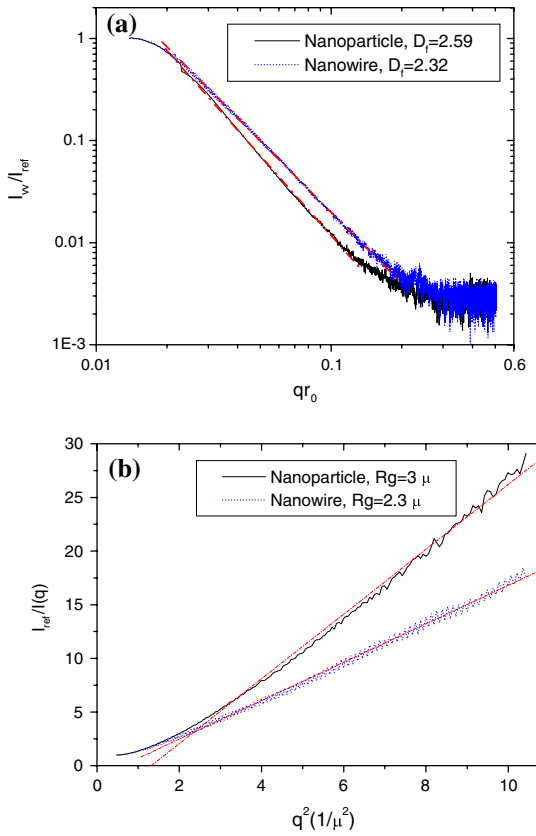

Fig. 5 (**a**). Determination of fractal dimension using small angle static light scattering. Aggregates of WO_3 irregular nanoparticles (lower curve) and uneven nanowires (upper curve) in EtOH. (**b**). R_g for aggregates of irregular WO_3 nanoparticles and uneven nanowires in EtOH. Linear fits (dash-dot) are for data points between $\theta = 6°$–$14°$

yield $R_g = 3$ μm and $R_g = 2.3$ μm for nanoparticles and uneven nanowires, respectively. Here we have adopted the use of I_{ref} representing the value at $I_{vv}(\theta = 3°)$ to consistently compare results of scattering from all aggregates investigated in this study. An important concern with Fig. 5b is the apparent exponential behavior of the curves at first few q data points. This, again, is related to the PMT saturation at smaller scattering angles encountered in *continuous* measurements, which delays the precipitous decline in $I(q)$ relative to I_{ref}. Guinier analyses based on incremental measurements on the same samples at later times (not shown) were always situated above the continuous measurements (e.g., see Fig. 7b below), and have shown linear behaviors extending to the low q values. The plots in Fig. 5b should not be considered as the most proper way of determining R_g,

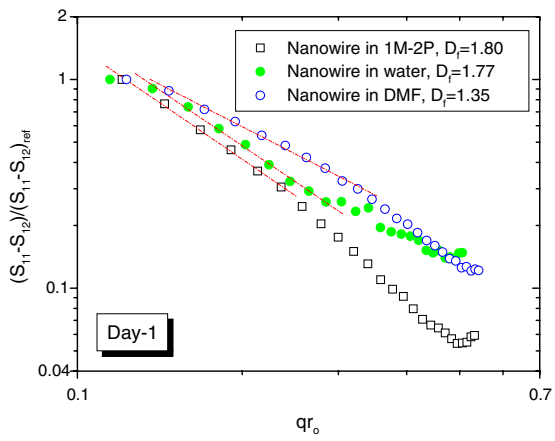

Fig. 6 Determination of fractal dimension using elliptically polarized light scattering. Aggregates of 2 μm average length bundled WO_3 nanowires in 1-methoxy-2-propanol (1M-2P), water and N,N-dimethylformamide (DMF) on Day-1. Linear fit is for incremental data points between $\theta = 25°$–$50°$, $\theta = 30°$–$65°$ and $\theta = 30°$–$70°$, respectively

but still serve as valuable indication of relative sizes, and provide practical information.

It is also possible to ensure a linear behavior at small q values in $I_{ref}/I(q)$ plot, and even extend it to higher q by using samples with slightly higher particle concentrations (e.g., $f_v \sim 10^{-5}$, not shown) in the light scattering measurements. This will result in higher scattered intensities at side angles (isotropic scattering) due to increased number of particles at the small end of particle size distribution. However, we present here the results corresponding to volume fractions in the order of $f_v \sim 10^{-6}$ for better comparisons between different measurements.

EPLS measurements on bundled WO_3 nanowires in three different solvents all with 0.1 wt.% nanowire content were performed after the calibration of the setup. Samples from 1-methoxy-2-propanol, distilled water and N,N-dimethylformamide suspensions were diluted to volume fractions $f_v = 0.6 \times 10^{-6}$, 0.8×10^{-6}, and 0.7×10^{-6}, respectively. Measurements of S_{11}–S_{12} normalized by the highest value at $\theta = 25°$ versus qr_o for the three samples are plotted in Fig. 6. To find the slope a linear fit was performed on incremental measurement data points between $\theta = 25°$–$50°$, $\theta = 30°$–$65°$ and $\theta = 30°$–$70°$, which yielded fractal dimensions of 1.80, 1.77, and 1.35 for WO_3 nanowires in 1-methoxy-2-propanol, distilled water and N,N-dimethylformamide, respectively.

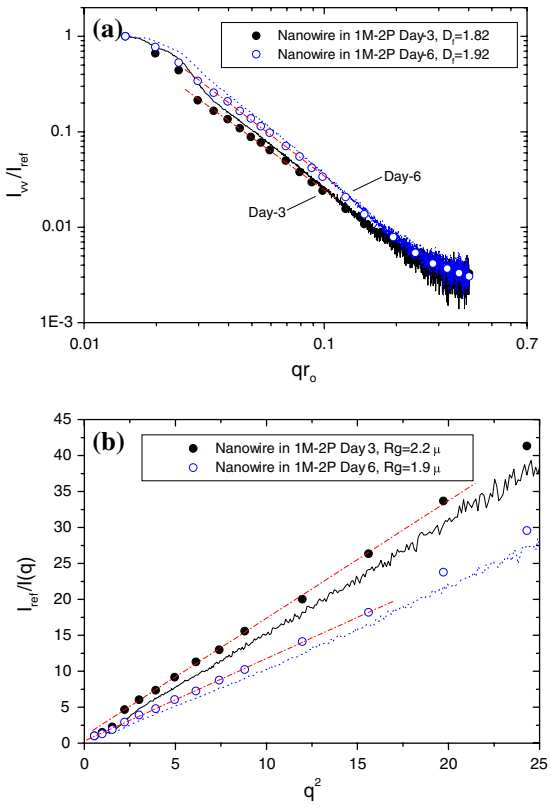

Fig. 7 (**a**). Determination of fractal dimension using small angle static light scattering. Aggregates of 2 μm average length bundled WO_3 nanowires in 1-methoxy-2-propanol (1M-2P) on Day-3 (solid line, solid circle) and Day-6 (dotted line, open circle). Linear fits (dash-dot) are for incremental data points between $\theta = 6°–20°$. (**b**). R_g for aggregates of 2 μm average length bundled WO_3 nanowires in 1-methoxy-2-propanol (1M-2P) on Day-3 (solid line, solid circle) and Day-6 (dotted line, open circle). Linear fits (dash-dot) are for data points between $\theta = 6°–18°$ and $\theta = 5°–16°$, respectively

The difference in fractal dimensions is the evidence to the effect of solvent rheological properties on aggregation behavior of WO_3 nanowires. All three suspensions were prepared from the products of the same nanowire synthesis. It should be emphasized, however, that due to the polydispersity of the nanowires and the consequent errors in pipetting, the samples might very well be biased towards a certain size distribution in one suspension than the other.

Therefore, rather than using the absolute values of the fractal dimensions reported above, their relative values should be emphasized as an indication of the effect of solvent type. The comparison of fractal dimensions clearly favors the use of N,N-dimethylformamide to obtain relatively open, linear aggregates of WO_3 nanowires. N,N-dimethylformamide has increased the stability of WO_3 nanowires in the suspension by reducing their tendency to form entangled, high fractal dimension aggregates. A similar value of fractal dimension ($D_f = 1.42$) found through numerical simulations was attributed to polarizable clusters as a result of aggregation on tips of aggregates (Jullien 1986).

Another important point that should be noted is that there is almost a 1-week time difference for bundled WO_3 nanowires between the time suspensions were prepared and any light scattering analysis were performed, which might have affected fractal dimension to some extent. This, however, is expected to be a minor effect, since WO_3 nanowires tend to have a slow aggregation rate even in extended periods of time as discussed in (Kozan and Mengüç 2007). Measurements on bundled WO_3 nanowires were repeated to detect possible changes in aggregate morphology with time. The measurements in Fig. 6 are labeled as Day-1.

Figure 7a shows normalized I_{vv} versus q measurements for bundled WO_3 nanowire aggregates in 1-methoxy-2-propanol at $f_v = 0.6 \times 10^{-6}$ carried out 2 days (labeled as Day-3) after the first measurements shown in Fig. 6. Solid lines corresponds to the average of two continuous measurements performed for scattering angles between $\theta = 3°–90°$. Experiments between the same scattering angles were repeated by performing the measurements at discrete scattering angles. It is apparent in Fig. 7a that the incremental measurement follows the trends of the continuous measurement except for a shift in intensity readings to lower values. Continuous measurements provide a good indication of the onset of different regimes, however, using incremental measurements provide more reliable estimates, and will be used when available.

On Day-3, $D_f = 1.82$ was found from the slope of the fractal scattering region by making a linear fit on data points between $\theta = 6°–20°$, a negligible increase within a 2 day period. Guinier analysis of the same measurements produced $R_g = 2.2$ μm from the linear fit between $\theta = 6°–18°$ as shown in Fig. 7b. $D_f = 1.92$ found on Day-6 from the slope between $\theta = 6°–20°$ as shown in the same figure proves that there is only a slight increase in fractal dimension of nanowire aggregates during the 6 day time span. Guinier analysis of the same measurements produced

R_g = 1.9 μm from the linear fit between θ = 5°–16° as shown in Fig. 7b. The slight decrease in R_g corresponds to a negligible change in spatial extent of nanowire aggregates in the same time period.

The increase in D_f does not necessarily point to the existence of a tendency of WO_3 nanowires to aggregate, but confirms the presence of restructuring of the aggregates in the suspension. Note that even though no shearing forces to complicate the structure were present for suspensions of bundled nanowires, restructuring may still have occurred due to van der Waals attraction. R_g, on the other hand, is an indication of the emergence of larger particles formed by aggregation and should be observed along with any increase in absolute values of forward scattered intensities to follow an aggregation process. Bundled WO_3 nanowire aggregates in 1-methoxy-2-propanol therefore seem to breakup at the outer branches to a small extent and turn into slightly more compact aggregates.

A similar test was done on bundled WO_3 nanowire aggregates in water with a higher initial suspension concentration of 0.5 wt.%. Two samples of WO_3 nanowire aggregates in water at $f_v = 1.3 \times 10^{-6}$ were prepared on Day-3 and Day-7 of the measurements, and the results are given in Table 2. On Day-3, D_f = 2.63 was found from the slope of the fractal scattering region and an increase to D_f = 2.74 was observed on Day-7. Guinier analysis of the same measurements produced R_g = 3.1 μm and R_g = 3.5 μm on Day-3 and Day-7, respectively. Unlike 1-methoxy-2-propanol, more compact aggregates were attained through an increase in size, i.e., aggregation, for bundled WO_3 nanowires in water.

Results of two other measurements performed on samples diluted from more concentrated suspensions on Day-3 are also tabulated in Table 2. Measurements performed for bundled WO_3 nanowire aggregates in 1-methoxy-2-propanol diluted to $f_v = 0.9 \times 10^{-6}$ was prepared from its suspension with an initial concentration of 0.7 wt.%. The sample in N,N-dimethylformamide diluted to $f_v = 1.0 \times 10^{-6}$ was prepared from its suspension of 0.4 wt.% initial concentration.

As mentioned before, even in the absence of shearing forces, van der Waals forces will ensure that particles will bond one another when brought close enough thus restructure the aggregate. In fact, high concentration suspensions reported above are potentially at a higher risk of undergoing restructuring due to increased probability of bonding. However, the higher initial suspension concentration does not seem to have a major effect on bundled WO_3 nanowires when 1-methoxy-2-propanol was used as the solvent. D_f = 1.86 and R_g = 1.8 μm on Day-3 (0.7 wt.%) given in Table 2 are very close to the results given in Fig. 7 (0.1 wt.%) on the same day. Similarly, linear structure of WO_3 nanowire aggregates were maintained with a higher storing concentration (0.4 wt.%) in N,N-dimethylformamide, with D_f = 1.43 on Day-3 compared to D_f = 1.35 in Fig. 6 (0.1 wt.%). Therefore, storing bundled WO_3 nanowires at higher suspension concentrations presented in this study does not universally cause an increase in fractal dimension or aggregate size. Note that, although fractal dimension for nanowire aggregates was the lowest in N,N-dimethylformamide, the aggregate size (R_g = 2.6 μm) was between those

Table 2 Summary of fractal properties of WO_3 nanoparticle and nanowire aggregates

WO_3 Sample	Solvent	Initial wt.%	D_f (or Slope)	R_g, μm
Nanoparticle	Ethanol	1.0	2.59	3
2 μm (Uneven)	Ethanol	1.0	2.32	2.3
2 μm (Bundled) Day-1[+]	1M-2P	0.1	1.80	–
2 μm (Bundled) Day-3[+]	1M-2P	0.1	1.82	2.2
2 μm (Bundled) Day-6[+]	1M-2P	0.1	1.92	1.9
2 μm (Bundled) Day-3[+]	1M-2P	0.7	1.86	1.8
2 μm (Bundled) Day-1[+]	DMF	0.1	1.35	–
2 μm (Bundled) Day-3[+]	DMF	0.4	1.43	2.6
2 μm (Bundled) Day-1[+]	Water	0.1	1.77	–
2 μm (Bundled) Day-3[+]	Water	0.5	2.63	3.1
2 μm (Bundled) Day-7[+]	Water	0.5	2.74	3.5
4 μm (Single)	Isopropanol	0.1	–7.48	–
6 μm (Single)	Isopropanol	0.1	–6.63	–
Nanoparticle Day-1	Acetone	0.5	2.52	3.7
Nanoparticle Day-2	Acetone	0.5	2.58	3.9
Nanoparticle Day-3	Acetone	0.5	2.62	3.8
Nanoparticle Day-6	Acetone	0.5	2.57	3.7
10 μm (Single) Day-1	Acetone	0.5	–6.28	–
10 μm (Single) Day-2	Acetone	0.5	–7.94	–
10 μm (Single) Day-3	Acetone	0.5	–6.75	–
10 μm (Single) Day-6	Acetone	0.5	–5.23	–

[+] Measurements performed approximately one week after suspension was prepared

obtained with 1-methoxy-2-propanol or water as solvents.

Figure 8 shows I_{vv} versus q measurements performed for single WO_3 nanowires of 4, 6, and 10 μm average length between $\theta = 3°–90°$. Measurements for 2 μm average length nanowires of Fig. 5a are also plotted on the same figure for comparison. The 4 and 6 μm WO_3 nanowires were diluted with isopropanol to $f_v = 0.6 \times 10^{-6}$ and 0.3×10^{-6}, respectively, and had an initial concentration of 0.1 wt.% before dilution. 10 μm WO_3 nanowires were suspended in acetone at $f_v = 1.1 \times 10^{-6}$. Initial concentration was 0.5 wt.% before dilution.

A linear fit performed on incremental data points for 4 μm WO_3 nanowires gives *Slope* = –7.48 between $\theta = 7°–10°$, for 6 μm WO_3 nanowires gives *Slope* = –6.63 between $\theta = 6°–9°$, and for 10 μm WO_3 nanowires gives *Slope* = –6.28 between $\theta = 5°–8°$. Continuous measurements give similar slopes within similar ranges of scattering angle: *Slope* = –7.54, –6.84, and –5.52 (between $\theta = 6°–10°$, $\theta = 6°–10°$, and $\theta = 5°–12°$) for 4, 6, and 10 μm WO_3 nanowires, respectively. Aggregates of WO_3 nanowires of high aspect ratios (those with average lengths that are longer than 2 μm) do not lend themselves to experimental determination of the fractal dimension and radius of gyration.

Measurements were also performed to detect possible changes in aggregate morphology of single WO_3 nanowires of 10 μm average length with time.

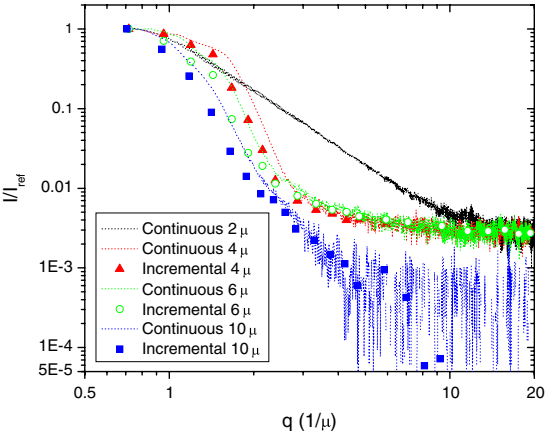

Fig. 8 Small angle static light scattering measurements for aggregates of 2, 4, 6, 10 μm WO_3 single nanowires. Linear fits (not shown) for incremental data points between $\theta = 7°–10°$, $\theta = 6°–9°$, and $\theta = 5°–8°$ give *Slope* = –7.48, *Slope* = –6.63, and *Slope* = –6.28 for 4, 6, and 10 μm nanowires, respectively

Table 2 presents results of measurements carried out in a span of 6 days between $\theta = 3°–90°$ on aggregates of these nanowires and a second sample of irregular WO_3 nanoparticles (Aldrich, Inc.), both suspended in acetone at $f_v = 1.1 \times 10^{-6}$. Initial concentrations of both samples were 0.5 wt.%. Our measurements show only minor differences scattering profiles in the span of 6 days of measurements. Note that, the D_f ($\sim$2.6) and R_g ($\sim$3.8 μm) for irregular nanoparticle aggregates were found through *incremental* measurements and can be used with greater degree of confidence. We believe these observations demonstrate the presence of a low level of aggregation of the 10 μm nanowires, along possibly with a slight change in fractal geometries due to restructuring induced by stirring of the suspensions. We used analytical and quasi-experimental models to determine the fractal dimensions of aggregates of 4, 6, and 10 μm nanowires in (Kozan and Mengüç 2007).

Conclusions

We have shown quantitatively that the solvent rheological properties result in different aggregation characteristics for the bundled WO_3 nanowires studied. Of all the three solvents used to suspend bundled WO_3 nanowires, N,N-dimethylformamide produced the most linear structure, although the aggregates were intermediate in size (in terms of R_g) when compared to those obtained with water and 1-methoxy-2-propanol. 1-methoxy-2-propanol, too, created an open structure (though not as linear as with N,N-dimethylformamide), but provided the smallest aggregate size, indicating a small tendency for aggregation. Water causes dramatically more compact aggregates and the highest aggregate size, and as such would not provide well-dispersed, stable suspensions.

The aggregate structures created by 1-methoxy-2-propanol could be visualized as to be in the form of snow flakes. In a suspension the snow flakes coagulate with one another (cluster-cluster aggregation) to create a somewhat high D_f ($\sim$1.80 on Day-1 to $\sim$1.92 on Day-6, no stirring). The increase in fractal dimension shows that these bonds are fragile so as to break, for example, during sampling. Thus the size of nanowire aggregates decreases ($R_g \sim 2.2$ μm on Day-3 to $\sim$1.9 μm on Day-6).

The aggregate structures created by N,N-dimethylformamide could be visualized to consist of bundles of wires like a bunch of pencils (but not all are perfectly aligned). The D_f is small (1.35–1.43), and the cluster *looks* linear as a result of aggregation on tips of aggregates which could be attributed to "polarizable" nanowire clusters. R_g is relatively high ($\sim$2.6 μm), as the bundle is large in extent. The closed structures formed in water, on the other hand, do not break up easily. They are more entangled and round, and in time clustered together to form even larger R_g. However, storing the nanowires at higher suspension concentrations for the values presented in this study does not universally cause an increase in fractal dimension or aggregate size.

We have also shown quantitatively that the different primary particle geometries of irregular nanoparticles and nanowires result in different aggregation characteristics. Aggregates of WO_3 nanoparticles are more compact and almost spherical in shape ($D_f \sim 2.6$), whereas the aggregates of 2 μm average length WO_3 nanowires with large uneven diameters ($\sim$200 nm) are more open, although still with a considerably high fractal dimension ($D_f \sim 2.3$). Similarly, comparing the extent of the aggregates, the initial R_g were considerably larger for nanoparticles ($\sim$3.8 μm) than for uneven nanowires ($\sim$2.3 μm).

Although measurements on aggregates of 10 μm single WO_3 nanowires did not allow experimental determination of R_g and D_f, experimental slopes revealed a low level of aggregation in the same period of time. Similar limitations were encountered for other nanowires longer than 2 μm, however, distinct scattering intensity profiles were observed for aggregates formed by single WO_3 nanowires of 4, 6, and 10 μm average length.

Acknowledgements MK is grateful to TUBITAK, Ankara, Turkey for their financial support (NATO A-1 scholarship). MK and MPM acknowledge the help of Dr. M. M. Aslan in the early phase of this work.

References

Aslan MM, Crofcheck C, Tao D, Mengüç MP (2006) Evaluation of micro-bubble size and gas hold-up in two-phase gas–liquid columns via scattered light measurements. J Quant Spectrosc Radiat Transf 101:527–539

Brasil AM, Farias TL, Carvalho MG (1999) A recipe for image characterization of fractal-like aggregates. J Aerosol Sci 30(10):1379–1389

Brasil AM, Farias TL, Carvalho MG, Koylu UO (2001) Numerical characterization of the morphology of aggregated particles. J Aerosol Sci 32(4):489–508

Bushell GC, Yan YD, Woodfield D, Raper J, Amal R (2002) On techniques for the measurement of the mass fractal dimension of aggregates. Adv Colloid Interface Sci 95(1):1–50

Chen Q, Saltiel C, Manickavasagam S, Schadler LS, Siegel RW, Yang H (2004) Aggregation behavior of single-walled carbon nanotubes in dilute aqueous suspension. J Colloid Interface Sci 280:91–97

Deepak FL, Saldanha P, Vivekchand SRC, Govindaraj A (2006) A study of the dispersions of metal oxide nanowires in polar solvents. Chem Phys Lett 417:535–539

Dimon P, Sinha SK, Weitz DA, Safinya CR, Smith GS, Varady WA, Lindsay HM (1986) Structure of aggregated gold colloids. Phys Rev Lett 57(5):595–598

Filippov AV, Zurita M, Rosner DE (2000) Fractal-like aggregates: relation between morphology and physical properties. J Colloid Interface Sci 229(1):261–273

Govindan R, Manickavasagam S, Mengüç MP (1995) On measuring the mueller matrix elements of soot agglomerates. Paper read at Radiation-I: proceedings of the first international symposium on radiative heat transfer. Kusadasi, Turkey: Begell House, NY, 1995

Hou FY, Wang W, Guo HT (2006) Effect of the dispersibility of zro2 nanoparticles in ni-zro2 electroplated nanocomposite coatings on the mechanical properties of nanocomposite coatings. Appl Surf Sci 252(10):3812–3817

Jullien R (1986) A new model of cluster aggregation. J Phys A Math Gen 19:2129–2136

Kozan M (2007) Characterization of nanoparticles using light scattering techniques. PhD dissertation, Mechanical Engineering Department, University of Kentucky, Lexington, KY

Kozan M, Mengüç MP (2007) Exploration of fractal nature of wo3 nanowire aggregates. J Quant Spectrosc Radiat Transfer (in press)

Lee CS, Lee JS, Oh ST (2003). Dispersion control of fe2o3 nanoparticles using a mixed type of mechanical and ultrasonic milling. Mater Lett 57(18):2643–2646

Mengüç MP, Manickavasagam S (1998) Characterization of size and structure of agglomerates and inhomogeneous particles via polarized light. Int J Eng Sci 36:1569–1593

Modest MF (1993) Radiative heat transfer. McGraw-Hill, Inc., New York

Nicolosi V, Vrbanic D, Mrzel A, McCauley J, O'Flaherty S, Mihailovic D, Blau WJ, Coleman JN (2005) Solubility of mo6s4.5i4.5 nanowires. Chem Phys Lett 401(1–3):13–18

Raper JA, Amal R (1993) Measurement of aggregate fractal dimensions using static light-scattering. Part Part Syst Characterization 10(5):239–245

Saltiel C, Chen Q, Manickavasagam S, Schadler LS, Siegel RW, Mengüç MP (2004) Identification of the dispersion behavior of surface treated nanoscale powders. J Nanopart Res 6(1):35–46

Saltiel C, Manickavasagam S, Mengüç MP, Andrews R (2005) Light-scattering and dispersion behavior of multiwalled carbon nanotubes. J Opt Soc Am A 22(8):1546–1554

Sorensen CM (1997) Scattering and absorption of light by particles and aggregates.In: Birdi KS (ed) Handbook of surface and colloid chemistry. CRC Press LLC, pp 533–558

Sorensen CM (2001) Light scattering by fractal aggregates: a review. Aerosol Sci Technol 35(2):648–687

Thangala J, Vaddiraju S, Bogale R, Thurman R, Powers T, Deb B, Sunkara MK (2007) Large-scale, hot-filament-assisted synthesis of tungsten oxide and related transition metal oxide nanowires. Small 3(5):890–896

Vaddiraju S, Chandrasekaran H, Sunkara MK (2003) Vapor phase synthesis of tungsten nanowires. J Am Chem Soc 125(36):10792–10793

Vincze A, Fata R, Zrinyi M, Horvolgyi Z, Kertsz J (1997) Comparison of aggregation of rodlike and spherical particles: a fractal analysis. J Chem Phys 18(8):7451–7458